

Article

A Fiber Optic Fabry–Perot Cavity Sensor for the Probing of Oily Samples

Vasileia Melissinaki ^{1,2}, Maria Farsari ¹ and Stavros Pissadakis ^{1,*}

¹ Foundation for Research and Technology-Hellas (FORTH), Institute of Electronic Structure and Laser (IESL), P.O. Box 1385, 71110 Heraklion, Greece; melvas@iesl.forth.gr (V.M.); mfarsari@iesl.forth.gr (M.F.)

² Department of Physics, University of Crete, 71003 Heraklion, Greece

* Correspondence: pissas@iesl.forth.gr; Tel.: +30-2810-391348

Academic Editors: Torsten Frosch and Stephen C. Bondy

Received: 3 September 2016; Accepted: 23 December 2016; Published: 3 January 2017

Abstract: A micro-optical Fabry–Perot cavity fabricated by non-linear laser lithography on the endface of a standard telecom fiber is tested here as a microsensor for identifying oily liquids. The device operates within the 1550 nm spectral region, while the spectra recorded in reflection mode correlate to the refractive index of the oily liquids used, as well as, to the diffusion dynamics in the time domain of the oily samples inside the porous photo-polymerized sensing head. The operation of the microresonator sensing probe is explained by using a three-layer Fabry–Perot model and basic diffusion physics to estimate diffusivities for three series of refractive index matching oils with different chemical compositions that had been used in those experiments. The distinct spectro-temporal response of this sensing probe to the different oil samples is demonstrated and discussed.

Keywords: optical fiber sensors; Fabry–Perot resonators; porous surfaces; oils; diffusion in porous layers; direct laser writing; multi-photon polymerization

1. Introduction

There is increased academic and industrial interest in the development of optical fiber sensing devices with direct implementation into the high socio-economical impact value chains of food quality monitoring, including taste monitoring, detection of adulteration, genetic modification and micro-organism growth [1–3]. The small size of optical fibers, their capability of providing intrusive sensing operation [4–6], and their straightforward interrogation in spectral or amplitude mode [7], has prompted further investigation into their use in functional sensing schemes covering the above horizontal and vertical applications. While the sensitivity of such types of photonic sensors is always the first parameter to be considered—usually expressed as wavelength shift of nm/RIU (RIU: refractive index units), corresponding to specific spectral features of the sensor monitored—, one parameter that predominantly affects the practical implementation of those sensors and their potential commercialization is selectivity. Selectivity of detection can be achieved through specific approaches based on chemisorption, biofunctionalized markers, electro-chemical reactions or swelling effects induced by in-diffusion processes [2,8–11]. In particular, in-diffusion processes are based on simple physisorption surface effects [12], influenced by the surface affinity and nano-structure of the sensing probe and the temperature of the analyte, while providing the advantage of simplicity in terms of the transduction mechanism.

We have recently demonstrated a micro-optical, hollow cavity, Fabry–Perot (FP) resonator accommodated onto the endface of a standard optical fiber for the high sensitivity tracing of organic volatile substances, while exhibiting high sensitivity (down to 4 parts per million (ppm)) and

specific selectivity capabilities [13,14]. This sensing probe was readily fabricated using multi-photon polymerization laser processing, a method providing high fabrication flexibility, sub-micrometric spatial resolution structuring and rapid prototyping characteristics. This sensing micro-probe was tested against the vapors of different chlorinated methylenes, exhibiting distinct spectro-temporal response to vapors of different chlorine coordination/number.

The results of these experiments demonstrate that the specific sensing head has specific advantages compared to the existing art. In comparison with other fiber-optic Fabry–Perot refractive index sensors, which are fabricated by combining standard optical fibers and microstructures optical fibers (MOFs) [15–17]; or by using laser micromachining [18,19], the present sensing head offers an intrinsic distinct transduction mechanism based on its porous surface facilitating the specie diffusion process. As investigated before, its distinct sensing behavior based on physisorption phenomena, allows full recovery after each sensing cycle and is reused several times without reducing its sensitivity and selectivity, always compared to sensors that are based on chemisorption effects [20–23].

Herein, we are extending the operation of this optical fiber endface, Fabry–Perot sensing probe, into the refractive index and substance-dependent sensing of oily liquids. The results presented below show that beyond the typical refractive index sensing capabilities of this sensor, monitored as corresponding wavelength shifts of the Fabry–Perot spectral notches, there is also a clear spectro-temporal feature related to the diffusion of the oily liquids inside a thin porous layer of the photo-polymerized cavity section. This spectro-temporal feature is manifested as a wavelength shift of the Fabry–Perot spectral notches, with typical time scales spanning between 5 and 35 min, depending on the chemical substances that the oily matrix used contains. By assuming a thin diffusion layer (where the oily medium can penetrate) and using a simple diffusion equation, we estimated diffusion constants for oils of different carrier materials and refractive index tuning additives. Therefore, the novelty of the sensor presented is the exploitation of the porosity of the photopolymerised Fabry–Perot light resonance structure, for monitoring the diffusion process of oily media into its volume, and accordingly recording the speed of this in-volume diffusion of the oil samples by interrogating modifications into the spectra of the Fabry–Perot resonator. Finally, the spectro-temporal data obtained are discussed using a three-layer Fabry–Perot model, for understanding the role of the thin porous layer underlying the particular transduction behavior of this optical sensing probe.

We believe that the sensing results presented in this work can constitute a first but solid basis for the development of simple, easily interrogated and functional, optical fiber sensing probes for the identification of adulteration processes in oily media [24,25]. Such a sensor can primarily target the high market volume of olive oil, which is considered to be the absolute standard with respect to the edible oils, with a proven positive impact on a balanced diet and prominent benefits to cardiovascular health [26,27]. Adulterants may be introduced in edible olive oils in ratios between 1% and 80% per weight [28,29]. Other substances that can affect the quality of olive oil are those of plasticizers in relation with the storing container or the condition of the specimen [30,31]. Both adulterants and plasticizers can be manifested in changes of the refractive index, optical absorption and physisorption properties of the oily medium. The sensor presented here can measure changes related to the refractive index and diffusion into a porous layer, for different compositions of refractive index oils that were examined. Other possible applications of the present sensing head include the classification of engine lubrication oils with respect to what the additives contain, the identification of possible regeneration processing [32]; or tracing of adulteration in cosmetic oils [33].

2. Materials and Methods

The sensing probe was fabricated on a standard telecom optical fiber, SMF-28e, using the two-photon polymerization process described in depth in previous work of the authors [13]. The photopolymerized matrix was based on an organic–inorganic hybrid composite [13,34], previously used for the fabrication of the “prism-like” microstructure suspended on pillars, attached onto the endface of the cleaved fiber. This optical architecture allows the formation of a small hollow cavity,

between the fiber endface and the photo-polymerized microstructure, which acts as a FP resonator, providing interrogation capabilities of the intermediate optical medium.

The design of the optical fiber sensor is shown schematically in Figure 1a, while Figure 1b presents an optical microscope image of the fabricated sensing head and finally Figure 1c shows the interference spectrum of the resonance probe under ambient air. In order to avoid multiple FP resonations, a 20° inclination is introduced in the outer reflection surface. This inclination directs the reflected light of the outer surface, outside of the numerical aperture of the fiber used; thus, interference effects related to this surface are fully suppressed, resulting in single FP interrogation spectra. A detailed description of the operation principle and the capabilities, as well as the fabrication technique of this endface FP sensing probe is presented in depth in reference [13]. The FP device has been optimized for operation in the spectral region lying between 1440 and 1660 nm, while being interrogated in reflection mode using a 50/50 AFC/PC optical fiber coupler. Measurements were performed using a superluminescence source and an optical spectrum analyzer (OSA) ANDO AQ6317B (ANDO, Japan) (Figure 2).

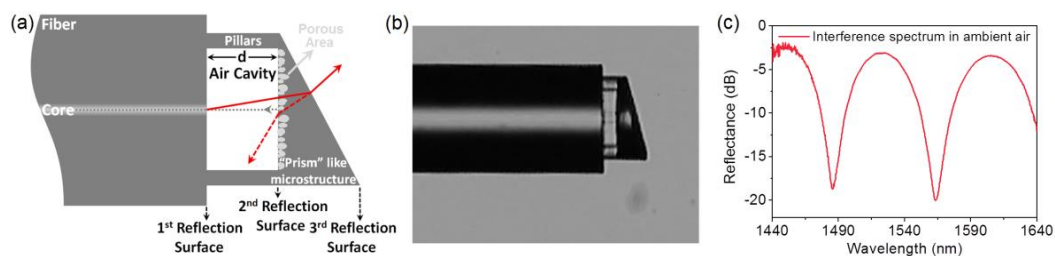


Figure 1. (a) Design of the FP microprism resonator onto the endface of the SMF-28e fiber. Grey dashed line corresponds to the reflected light that is recording, while red solid line and red dashed line correspond to the guided light for the maximum angle of the Numerical Aperture (NA) of the core and the reflected light from the outer surface of the microstructure respectively. The porous area on the second reflection surface is also presented with light grey “dots”; (b) Optical microscope image of the fabricated microprism resonator; (c) Interference spectrum on the resonant probe in ambient air conditions.

In order to investigate the sensitivity of the fabricated optical fiber sensing device at the changes of the refractive index inside the microcavity, as well as its surface affinity due to the fabricated porous membrane and how this might be affected due to the filling of the pores by liquid materials with different characteristics (i.e., chemical composition, viscosity), the FP sensing probe was tested by using different series of refractive index oils. Three different series of refractive index liquids were used for these experiments, namely SERIES AA, the refractive indices of which range between $n_D = 1.400$ – 1.458 ; SERIES A₁ with $n_D = 1.460$ – 1.570 ; and finally SERIES A₂ $n_D = 1.572$ – 1.640 (see Table 1). All the aforementioned refractive index liquids were purchased from Cargille Laboratories, Cedar Grove, NJ, USA. Information about the exact ratios between the substances used in these refractive index matching oils were not disclosed by the manufacturing company.

Table 1. Series of Cargille refractive index liquids that were used for the experiments.

Refractive Index Liquid Series	First Basic Substance	Second Basic Substance	Refractive Indices Range (n_D)
SERIES AA	Mixture of Aliphatic/Alicyclic Hydrocarbons	—	1.400–1.458
SERIES A1	Mixture of Aliphatic/Alicyclic Hydrocarbons	Hydrogenated Terphenyl	1.460–1.570
SERIES A2	Hydrogenated Terphenyl	1-Bromonaphthalene	1.572–1.640

A simple set-up was used in order to characterize the response of the sensing head to these refractive index oils (Figure 2). Some droplets of the desirable oil were drop-casted on a microscope slide which was lying on the experiment table. The optical fiber sensing head was immersed in the oil and the FP resonance spectra were recorded in real time, i.e., every 2.5 min, while the microcavity of the sensing head and as a consequence, the pores of the fabricated membrane, were getting filled with the oil. All measurements were performed at an ambient temperature of 21.5 °C, while the sensing behavior of the probe was tested up to 32.5 min after its exposure to the refractive index oils.

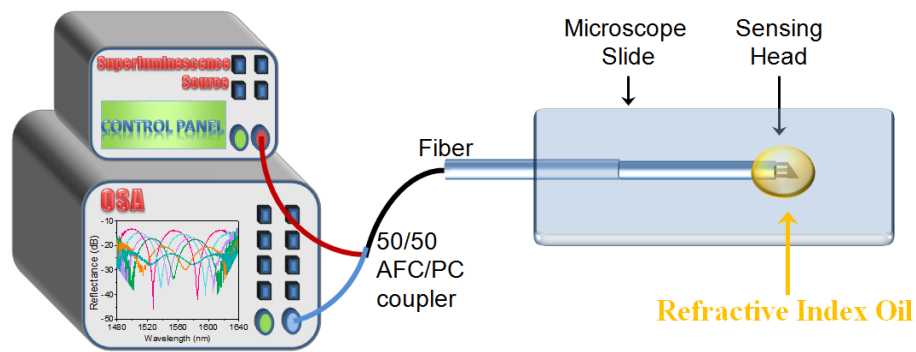


Figure 2. Experimental set-up for Cargille refractive index liquids measurements.

All the series of the Cargille refractive index liquids were measured, with the step between the refractive index changes from the one oil to the other being 0.01 (e.g., 1.40, 1.41, 1.42 etc.). After measuring each one of the oils, the sensing head was immersed in 2-propanol for 5 min in order to rinse the refractive index oil and the microcavity to be cleaned for the next measurement. Then, the sensing head was left drying in ambient air for approximately 30 min before the next set of measurements was started. In all measurements performed, the same sensing head was used, showing no spectral hysteresis/distortion after repeated oil immersion and isopropanol cleaning process.

3. Results and Discussion

The wavelength shift versus immersion time in the oily samples, of the 1563 nm notch of the FP resonator for three oils with the lowest refractive indices from the series AA, A1 and A2 are shown in Figure 3.

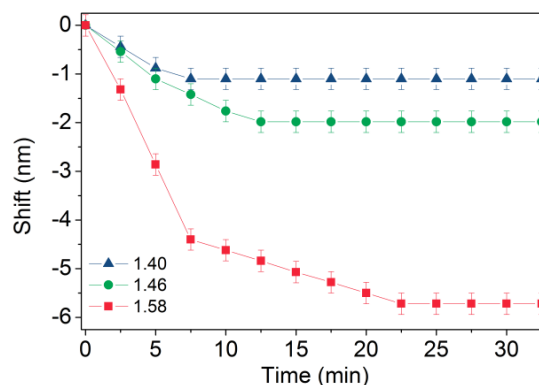


Figure 3. Wavelength shift versus immersion time in the oily sample, of the 1563 nm notch of the FP resonator for three oils with the lowest refractive indices from the series AA, A1 and A2. The error bars present the resolution of the optical spectrum analyzer during the recording of the measurements.

Figure 4 presents the strength visibility of the fringes versus the refractive index for all the refractive index oily liquids that had been examined from series AA, A1 and A2. In the case that the

refractive index of the oily liquid approximates the refractive index of one of the optical materials constituting the FP cavity (RI of first reflection surface $n_{\text{core}} = 1.4682$, while RI of first reflection surface $n_{\text{prism}} = 1.52$) the fringe visibility reaches values close to zero; at those turning points, Fresnel's reflections at the corresponding interface almost vanish.

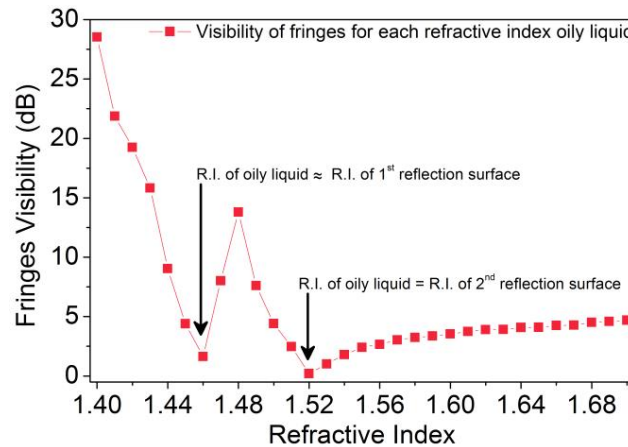


Figure 4. Strength visibility of the fringes versus the refractive index of the oily liquids that were examined.

Similar spectro-temporal sensing results presented in Figure 3 are also presented for refractive index oils from one series (that of A1) in Figure 5a; a contour graph of the wavelength shift of a single FP notch is presented in Figure 5b. The results of Figures 3 and 5a reveal that either oils of different compositions and substances, or oils from the same composition but of different ratios of substances, exhibit different temporal behavior with respect to the FP notch wavelength shifts. We attribute this time-dependent spectral behavior to the diffusion effects occurring within the photopolymerized material constituting one of the reflective surfaces of the FP resonator. Previous investigations have shown that two-photon photopolymerized materials exhibit a surface roughness of the order of 30 nm; this rough surface layer constitutes a place where oil diffusion effects can take place [35]. This temporal varying effect has been observed before in our FP sensing system for chlorinated organic vapors stimulation (although of more complex dynamics) [14]. The behavior presented here follows a monotonic blue shift trend reaching a plateau of wavelength shift of the FP fringes after characteristic times of a few tens of minutes. Accordingly, by considering only the maximum wavelength shift obtained from the sensing head used, a refractive sensitivity of 66 nm/RIU is obtained between the 1.50 and 1.51 refractive index oils.

Again, the data of Figures 3 and 5a refer to an experimentally measured quantity, that of the wavelength shift of the FP resonator notches, however, this does not constitute a direct physical quantity/parameter that can characterize the effect of the oil diffusion into the porous section of the photopolymerized prism. A first idea was the use of a penetration depth of the oil into the porous section, versus time; this approach suffers from complexity since both the penetration depth and the corresponding refractive index of it are considered unknown. A simpler approach is followed wherein we assume an average refractive index of the whole porous section, defined as n_{diffuse} . While this assumption does not describe in full detail the oil diffusion effect into the porous area, it provides a first insight into the physical effect, which can lead to an easy parametrization of the sensing mechanism.

Therefore, in order to explain the specific spectro-temporal behavior and predict the diffusion effects in the porous membrane of the fabricated sensing head, as described above, a three-layer Fabry–Perot description model is used. Such types of multilayer FP models have been used in our previous studies, for predicting the spectral shifts during the pores filling with the Cl-based volatile organic compounds, as well as the formation of the physisorption liquid layer on the reflection surface [14]. Herein, the three-layer model is applied in the data of the lowest refractive indices from

each series, for calculating the $n_{diffuse}$ refractive index within the porous layer, due to the diffusion of the oil in the pores of the reflection surface of the photopolymerized section.

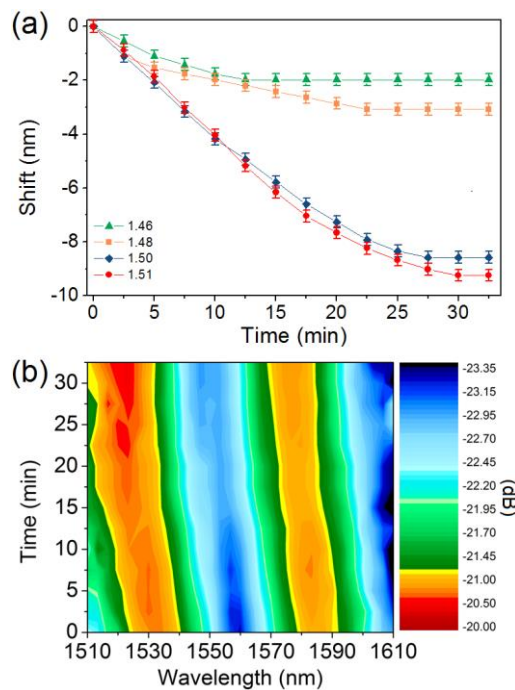


Figure 5. (a) Wavelength shift versus immersion time in the oily sample, of the 1563 nm notch of the FP resonator, for four oils with different refractive indices from series A1; (b) contour graph of the wavelength shift of a single FP notch for 1.51 refractive index oil. The error bars present the resolution of the optical spectrum analyzer during the recording of the measurements.

Initially, we divide the photopolymerized prism constituting the one reflection surface of the FP into two layers: an outer thin porous layer with dimension of the order of the roughness of the material (namely 30 nm), and a thick semi-continuum layer, nominally non-porous (Figure 6, inset schematic representation). Using the same three-layer model for air medium within the empty cavity of the FR resonator, the porosity of the thin porous layer is translated as a porous refractive index; in the present case, this porous refractive index was estimated to be $n_{pores} = 1.26$, while introducing a filling factor G of 0.5 describing the porosity of the thin diffusion layer [14].

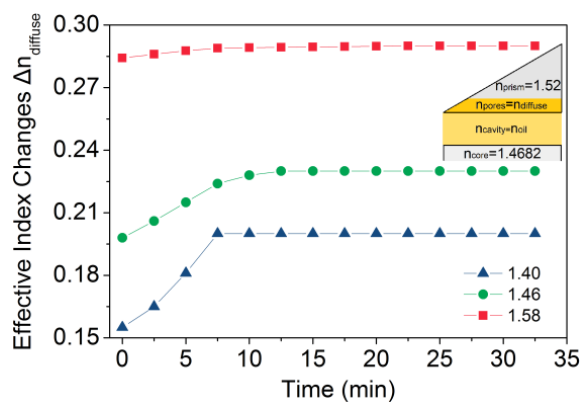


Figure 6. Effective index changes versus immersion time in the oily sample, for three oils with the lowest refractive indices from the series AA, A1 and A2. The refractive indices that were used for the applied three-layer FP theoretical model are presented in the inset schematic representation (see text).

Assuming that by the immersion of the sensing head in the refractive index oil, the refractive index of the open cavity is equal to that of the used oil $n_{\text{cavity}} = n_{\text{oil}}$, the average refractive index n_{diffuse} of the infiltrated porous thin layer can be calculated for each measurement that was recorded during the time, until the porous layer is fully-filled and the wavelength shift reaches the plateau. The changes of the n_{diffuse} versus immersion time into the oil were calculated from the above theoretical model are presented in Figure 6, by taking $\Delta n_{\text{diffuse}} = n_{\text{diffuse}} - n_{\text{pores}}$. A first quantification of the diffusion is done by fitting the refractive index data of Figure 5 using an error function of the form:

$$f(t) = A + B \times \text{erf}(t/t_{\text{Ch}}) \quad (1)$$

where t_{Ch} is the characteristic time of the oil diffusion into the sensing head, and A and B are constant factors. Equation (1) is the most commonly used error function for fitting diffusion data in order to calculate the characteristic time t_{Ch} that a liquid needs to penetrate into a porous medium. The estimation of the characteristic time t_{Ch} for each oil examined is then used in the approximate diffusion equation [36]:

$$d = \sqrt{2Dt_{\text{Ch}}} \quad (2)$$

where d is the diffusion length (in our case the thickness of the porous layer, namely 30 nm), D is the diffusion coefficient and t_{Ch} is the time that the liquid needs to penetrate and fill the length of the diffusion layer [37], namely, the characteristic time t_{Ch} . By using the t_{Ch} from the fitting of the error function to our data and Equation (2), the diffusivities for the three oils with the lowest refractive indices from the series AA, A1 and A2 were calculated to be, $D_{1.40} = 1.021 \times 10^{-14} \text{ cm}^2/\text{s}$, $D_{1.46} = 8.678 \times 10^{-15} \text{ cm}^2/\text{s}$ and $D_{1.58} = 8.870 \times 10^{-15} \text{ cm}^2/\text{s}$, respectively. Since the oily media used are of non-/low-polar nature, and do not react with the photopolymerized porous material, we consider the diffusivities estimated to be constant during the diffusion of the specimens into the porous area [38]. The diffusivity figures estimated here are greater than those observed for the diffusion of water in silica glass, which are $\sim 10^{-17} \text{ cm}^2/\text{s}$, at higher temperatures and at typical diffusion depths of the order of 10 nm. This is not a surprising finding, since the photopolymerized glass is of “softer” nature (porous surface, Young modulus $\sim 3 \text{ GPa}$), containing also organic modifiers [39]; the last may exhibit an improved affinity to the organic oils used in this study.

The above diffusivity data reveal that the addition of Hydrogenated Terphenyl (for its increased refractive index ~ 1.56) into the mixture of Aliphatic/Alicyclic Hydrocarbons (which are the basic substances for the AA series) for generating the series A1 of the index matching liquids used, introduces a slower diffusion of these oils into the porous photopolymerized matrix. Hydrogenated Terphenyl also has a high molecular weight ($\sim 238.36 \text{ g/mol}$) and a long triple aromatic hydrocarbon chain, facts which can render its diffusion through the porous sites of the FP sensing head slower. On the other hand, A2 series which is based on the Hydrogenated Terphenyl and the addition of 1-Bromonaphthalene—a halogenated aromatic hydrocarbon of the higher refractive index (~ 1.65) of all substances examined herein—marginally increases diffusion, possibly due to the polarity introduced by the bromide bond which can underline physisorption.

Summarizing the sensing data above, one can use the probe presented here for proceeding to an oil sensing protocol, while attributing two identification parameters to each oil sample: a characteristic wavelength shift depending upon its refractive index, and a characteristic relaxation time or diffusivity depending on the diffusion process into the photopolymerized section.

4. Conclusions

In this study, a simple and functional optical fiber endface Fabry–Perot sensor fabricated by multiphoton polymerization was presented for the probing of the substances of oily media with respect to their diffusion behavior in the porous reflection surface of the sensing head and refractometric behavior. Results reveal that each of the oily liquids—either coming from the same series or from the three different series that had been used herein—exhibits a distinct optical spectra signature versus

sensing time. Moreover, the findings are explained using a three-layer Fabry–Perot model, and by using simple diffusion physics, the diffusivity factor of each oily liquid into the organic–inorganic matrix is estimated.

Further summarizing, the characteristic and distinct wavelength shift profile—depending upon the refractive index of each Cargille refractive index oily liquid—and the characteristic relaxation time—depending on the diffusion process into the photopolymerized layer of the sensing head—can be used in order to proceed to an oil sensing protocol, for the development of simple, easily interrogated and functional, optical fiber sensing probes for the identification of adulteration processes in oily media such as olive oil.

The implementation of additional identification parameters per sample including the optical loss of the oil at a specific wavelength, as well as the use of temperature stimulus for speeding up diffusion times are currently under investigation.

Acknowledgments: This research has been co-financed by the European Union (European Social Fund—ESF) and Greek national funds through the Operational Program “Education and Lifelong Learning” of the National Strategic Reference Framework (NSRF)—Research Funding Program: THALES, Project 3DSET (MIS 380278). This work was also partially supported by the framework of “Quality of Life” project within the KRIPIS action of the General Secretariat of Research and Technology, funded by Greece and the European Regional Development Fund of the European Union under the Operational Programme Competitiveness and Entrepreneurship (NSRF 2007-2013) and the Regional Operational Programme of Crete & the Aegean Islands.

Author Contributions: S.P. and V.M. conceived and designed the experiments; V.M. performed the experiments, and M.F. supervised the photo-polymerization processing; V.M. and S.P. analyzed the data; V.M., M.F. and S.P. wrote the paper.

Conflicts of Interest: The authors declare no conflict of interest.

References

1. Abdelhaseib, M.U.; Singh, A.K.; Bailey, M.; Singh, M.; El-Khateib, T.; Bhunia, A.K. Fiber optic and light scattering sensors: Complimentary approaches to rapid detection of salmonella enterica in food samples. *Food Control* **2016**, *61*, 135–145. [[CrossRef](#)]
2. Candiani, A.; Sozzi, M.; Cucinotta, A.; Selleri, S.; Veneziano, R.; Corradini, R.; Marchelli, R.; Childs, P.; Pissadakis, S. Optical fiber ring cavity sensor for label-free DNA detection. *IEEE J. Sel. Top. Quantum Electron.* **2012**, *18*, 1176–1183. [[CrossRef](#)]
3. Mignani, A.G.; Ciaccheri, L.; Cucci, C.; Mencaglia, A.A.; Cimato, A.; Attilio, C.; Ottevaere, H.; Thienpont, H.; Paolesse, R.; Mastroianni, M.; et al. Eat-by-light: Fiber-optic and micro-optic devices for food quality and safety assessment. *IEEE Sens. J.* **2008**, *8*, 1342–1354. [[CrossRef](#)]
4. Desjardins, A.E.; Hendriks, B.H.W.; van der Voort, M.; Nachabe, R.; Bierhoff, W.; Braun, G.; Babic, D.; Rathmell, J.P.; Holmin, S.; Soderman, M.; et al. Epidural needle with embedded optical fibers for spectroscopic differentiation of tissue: Ex vivo feasibility study. *Biomed. Opt. Express* **2011**, *2*, 1452–1461. [[CrossRef](#)] [[PubMed](#)]
5. Liu, Y.; Gassino, R.; Braglia, A.; Vallan, A.; Perrone, G. Fibre probe for tumour laser thermotherapy with integrated temperature measuring capabilities. *Electron. Lett.* **2016**, *52*, 798–800. [[CrossRef](#)]
6. Frosch, T.; Yan, D.; Popp, J. Ultrasensitive fiber enhanced UV resonance raman sensing of drugs. *Anal. Chem.* **2013**, *85*, 6264–6271. [[CrossRef](#)] [[PubMed](#)]
7. Pevec, S.; Donlagic, D. Miniature fiber-optic sensor for simultaneous measurement of pressure and refractive index. *Opt. Lett.* **2014**, *39*, 6221–6224. [[CrossRef](#)] [[PubMed](#)]
8. Wang, X.-D.; Wolfbeis, O.S. Fiber-optic chemical sensors and biosensors (2013–2015). *Anal. Chem.* **2016**, *88*, 203–227. [[CrossRef](#)] [[PubMed](#)]
9. Carrasquilla, C.; Xiao, Y.; Xu, C.Q.; Li, Y.F.; Brennan, J.D. Enhancing sensitivity and selectivity of long-period grating sensors using structure-switching aptamers bound to gold-doped macroporous silica coatings. *Anal. Chem.* **2011**, *83*, 7984–7991. [[CrossRef](#)] [[PubMed](#)]
10. Park, C.S.; Han, Y.; Joo, K.I.; Lee, Y.W.; Kang, S.W.; Kim, H.R. Optical detection of volatile organic compounds using selective tensile effects of a polymer-coated fiber bragg grating. *Opt. Express* **2010**, *18*, 24753–24761. [[CrossRef](#)] [[PubMed](#)]

11. Fujiwara, Y.; Amao, Y. 1-pyrenedecanoic acid chemisorption film as a novel oxygen sensing material. *Sens. Actuator B* **2002**, *85*, 175–178. [[CrossRef](#)]
12. Widera, J.; Bunker, C.E.; Pacey, G.E.; Katta, V.R.; Brown, M.S.; Elster, J.L.; Jones, M.E.; Gord, J.R.; Buckner, S.W. Kinetic behavior of polymer-coated long-period-grating fiber-optic sensors. *Appl. Opt.* **2005**, *44*, 1011–1017. [[CrossRef](#)] [[PubMed](#)]
13. Melissinaki, V.; Farsari, M.; Pissadakis, S. A fiber-endface, Fabry-Perot vapor microsensor fabricated by multiphoton polymerization. *IEEE J. Sel. Top. Quantum Electron.* **2015**, *21*, 10. [[CrossRef](#)]
14. Melissinaki, V.; Konidakis, I.; Farsari, M.; Pissadakis, S. Fiber endface Fabry-Perot microsensor with distinct response to vapors of different chlorinated organic solvents. *IEEE Sens. J.* **2016**, *16*, 7094–7100. [[CrossRef](#)]
15. Villatoro, J.; Kreuzer, M.P.; Jha, R.; Minkovich, V.P.; Finazzi, V.; Badenes, G.; Pruneri, V. Photonic crystal fiber interferometer for chemical vapor detection with high sensitivity. *Opt. Express* **2009**, *17*, 1447–1453. [[CrossRef](#)] [[PubMed](#)]
16. Silva, S.; Roriz, P.; Frazão, O. Refractive index measurement of liquids based on microstructured optical fibers. *Photonics* **2014**, *1*, 516–529. [[CrossRef](#)]
17. Tian, J.J.; Lu, Y.J.; Zhang, Q.; Han, M. Microfluidic refractive index sensor based on an all-silica in-line Fabry-Perot interferometer fabricated with microstructured fibers. *Opt. Express* **2013**, *21*, 6633–6639. [[CrossRef](#)] [[PubMed](#)]
18. Ran, Z.L.; Rao, Y.J.; Liu, W.J.; Liao, X.; Chiang, K.S. Laser-micromachined Fabry-Perot optical fiber tip sensor for high-resolution temperature-independent measurement of refractive index. *Opt. Express* **2008**, *16*, 2252–2263. [[CrossRef](#)] [[PubMed](#)]
19. Wei, T.; Han, Y.K.; Li, Y.J.; Tsai, H.L.; Xiao, H. Temperature-insensitive miniaturized fiber inline Fabry-Perot interferometer for highly sensitive refractive index measurement. *Opt. Express* **2008**, *16*, 5764–5769. [[CrossRef](#)] [[PubMed](#)]
20. Some, S.; Xu, Y.; Kim, Y.; Yoon, Y.; Qin, H.; Kulkarni, A.; Kim, T.; Lee, H. Highly sensitive and selective gas sensor using hydrophilic and hydrophobic graphenes. *Sci. Rep.* **2013**, *3*, 1868. [[CrossRef](#)] [[PubMed](#)]
21. Konstantaki, M.; Klini, A.; Anglos, D.; Pissadakis, S. An ethanol vapor detection probe based on a zno nanorod coated optical fiber long period grating. *Opt. Express* **2012**, *20*, 8472–8484. [[CrossRef](#)] [[PubMed](#)]
22. Hlubina, P.; Kadulova, M.; Ciprian, D.; Sobota, J. Reflection-based fibre-optic refractive index sensor using surface plasmon resonance. *J. Eur. Opt. Soc. Rapid Publ.* **2014**, *9*, 14033. [[CrossRef](#)]
23. Villar, I.D.; Matias, I.R.; Arregui, F.J.; Claus, R.O. ESA-based in-fiber nanocavity for hydrogen-peroxide detection. *IEEE Trans. Nanotechnol.* **2005**, *4*, 187–193.
24. Coelho, L.; Viegas, D.; Santos, J.L.; de Almeida, J. Detection of extra virgin olive oil thermal deterioration using a long period fibre grating sensor coated with titanium dioxide. *Food Bioprocess Technol.* **2015**, *8*, 1211–1217. [[CrossRef](#)]
25. Biswas, P.; Basumallick, N.; Dasgupta, K.; Ghosh, A.; Bandyopadhyay, S. Application of strongly overcoupled resonant modes of long-period fiber gratings to measure the adulteration of olive oil. *Appl. Opt.* **2016**, *55*, 5118–5126. [[CrossRef](#)] [[PubMed](#)]
26. Covas, M.I.; Konstantinidou, V.; Fitó, M. Olive oil and cardiovascular health. *J. Cardiovasc. Pharmacol.* **2009**, *54*, 477–482. [[CrossRef](#)] [[PubMed](#)]
27. Covas, M.I. Olive oil and the cardiovascular system. *Pharmacol. Res.* **2007**, *55*, 175–186. [[CrossRef](#)] [[PubMed](#)]
28. Fragaki, G.; Spyros, A.; Siragakis, G.; Salivaras, E.; Dais, P. Detection of extra virgin olive oil adulteration with lampante olive oil and refined olive oil using nuclear magnetic resonance spectroscopy and multivariate statistical analysis. *J. Agric. Food Chem.* **2005**, *53*, 2810–2816. [[CrossRef](#)] [[PubMed](#)]
29. Dourtoglou, V.G.; Dourtoglou, T.; Antonopoulos, A.; Stefanou, E.; Lalas, S.; Poulos, C. Detection of olive oil adulteration using principal component analysis applied on total and regio fa content. *J. Am. Oil Chem. Soc.* **2003**, *80*, 203–208. [[CrossRef](#)]
30. Bi, X.; Pan, X.; Yuan, S.; Wang, Q. Plasticizer contamination in edible vegetable oil in a U.S. Retail market. *J. Agric. Food Chem.* **2013**, *61*, 9502–9509. [[CrossRef](#)] [[PubMed](#)]
31. Preedy, V.R.; Watson, R.R. *Olives and Olive Oil in Health and Disease Prevention*; Elsevier Science: Amsterdam, The Netherlands, 2010.
32. Abro, R.; Chen, X.; Harijan, K.; Dhakan, Z.A.; Ammar, M. A comparative study of recycling of used engine oil using extraction by composite solvent, single solvent, and acid treatment methods. *ISRN Chem. Eng.* **2013**, *2013*, 5. [[CrossRef](#)]

33. Jentzsch, P.; Ramos, L.; Ciobotă, V. Handheld Raman spectroscopy for the distinction of essential oils used in the cosmetics industry. *Cosmetics* **2015**, *2*, 162–176. [[CrossRef](#)]
34. Sakellari, I.; Kabouraki, E.; Gray, D.; Purlys, V.; Fotakis, C.; Pikulin, A.; Bityurin, N.; Vamvakaki, M.; Farsari, M. Diffusion-assisted high-resolution direct femtosecond laser writing. *Acs Nano* **2012**, *6*, 2302–2311. [[CrossRef](#)] [[PubMed](#)]
35. Malinauskas, M.; Zukauskas, A.; Purlys, V.; Belazaras, K.; Momot, A.; Paipulas, D.; Gadonas, R.; Piskarskas, A.; Gilbergs, H.; Gaidukeviciute, A.; et al. Femtosecond laser polymerization of hybrid/integrated micro-optical elements and their characterization. *J. Opt.* **2010**, *12*, 124010. [[CrossRef](#)]
36. Balluffi, R.W.; Allen, S.M.; Carter, W.C. The diffusion equation. In *Kinetics of Materials*; John Wiley & Sons, Inc.: Hoboken, NJ, USA, 2005; pp. 77–97.
37. Doremus, R.H. Diffusion of water in silica glass. *J. Mater. Res.* **1995**, *10*, 2379–2389. [[CrossRef](#)]
38. Shamiryan, D.; Baklanov, M.R.; Lyons, P.; Beckx, S.; Boullart, W.; Maex, K. Diffusion of solvents in thin porous films. *Colloids Surf. A* **2007**, *300*, 111–116. [[CrossRef](#)]
39. Riegel, B.; Kiefer, W.; Hofacker, S.; Schottner, G. Investigations on the organic crosslinking in ormocers by means of Raman spectroscopy. *Ber. Bunsen Ges. Phys. Chem. Chem. Phys.* **1998**, *102*, 1573–1576. [[CrossRef](#)]



© 2017 by the authors; licensee MDPI, Basel, Switzerland. This article is an open access article distributed under the terms and conditions of the Creative Commons Attribution (CC-BY) license (<http://creativecommons.org/licenses/by/4.0/>).